Supplemental Data

Microstate parameters

As microstates derived from analytic amplitude and phase signals have not been considered so far, we here give a summary of basic microstate statistics as used in (von Wegner et al., 2017, 2018). Table S1 gives the peaks-per-second (PPS) characteristic that counts the number of local maxima in the global field power time course of EEG data before ($PPS_{1\text{-}30}$) and after alpha band-pass filtering ($PPS_{8\text{-}12}$), where the subscripts indicate the underlying frequency band in [1/s]. As expected, 8-12 Hz band-pass filtering removes some high-frequency peaks and leads to slightly lower PPS values. Next, the global explained variance of PCA-derived microstates for 1-30 Hz data ($GEV_{1\text{-}30}$) shows values similar to those reported in the literature (Michel and Koenig, 2018). The GEV definition contains GFP-dependent weighting terms (Murray et al., 2008), and as GFP is computed from the oscillatory data, this weighting is only appropriate for oscillation-derived microstates. We therefore also provide non-weighted explained variance values for microstates computed from 1-30 Hz data ($EV_{1\text{-}30}$), alpha oscillations ($EV_{8\text{-}12}$), analytic alpha amplitudes (EV_A) and analytic alpha phases (EV_ϕ). Each value contains the total variance explained by the four corresponding microstates. In general, the non-weighted explained variances are larger than the GEV values and are similar for oscillatory, amplitude- and phase-microstates. All variances are expressed as %/100.

Table S2 contains further microstate parameters that summarize the distribution of the four microstate classes within each sequence and the properties of the transition matrix (matrix of transition probabilities) between each pair of microstates. As amplitude- and phase-derived microstates do not necessarily comply with the standard microstate map geometries labelled A-D in the literature (Michel and Koenig, 2018), we chose parameters that do not depend on the specific labeling (von Wegner et al., 2018).

The relative time covered by each microstate class in a given microstate sequence is proportional to the estimated probability of observing each mi-

crostate class. The Shannon entropy H of this probability distribution is a single non-negative number that summarizes the information about microstate probabilities in a label-independent manner (von Wegner et al., 2018). Using the natural logarithm ($\log_e$) in the definition of H, the unit of entropy is nats and the maximum value for $n = 4$ microstates is $H_{max} = \log_e 4 \approx 1.39$ nats.

Using the same approach of microstate label-independent metrics, we summarized transition matrices by their mixing time τ, i.e. the inverse of the difference between the two largest matrix eigenvalues (von Wegner et al., 2018). The mixing time has no physical unit but is determined by the sampling rate at which the transition matrix was calculated, in our case 250 Hz.

We observed that the Shannon entropies of alpha band microstates were only slightly smaller than those of 1-30 Hz microstates, meaning that the alpha band microstate distribution is less uniform than the distribution of full bandwidth microstates. Shannon entropy values for amplitude and phase microstate sequences lie within the same range as those for 1-30 Hz and 8-12 Hz oscillation-derived microstates.

Mixing times can be interpreted as a simple way of describing the initial decay of the AIF. The transition matrix describes the microstate sequence as a first-order Markov process (von Wegner et al., 2017) and the mixing time describes how fast this Markov process reaches its equilibrium distribution (von Wegner et al., 2018). Large values of τ correspond to a slow AIF decay, small values of τ (fast mixing) correspond to a quick decay. The last four columns of Table S2 show that 1-30 Hz, 8-12 Hz and analytic phase microstates all share a similar Markov structure, in terms of how fast they approach their respective equilibrium distributions, whereas the analytic amplitude microstates show much larger τ values, in accordance with the slow decay of the corresponding AIFs shown in Figure 6A and Figure 7B.

Amplitude and phase microstates

The supplemental Figure S1 exemplifies the similarity between EEG microstate map geometries computed from full bandwidth EEG data (A, 1-30 Hz)

and microstates derived from the alpha frequency band (B, 8-12 Hz) for a single subject. The following rows show the shape of microstates computed from the analytic alpha amplitude (C) and from the analytic alpha phase (D). The differences between the maps in A and B are mainly due to polarity, which has no effect during the microstate fitting procedure. The ordering of the microstates shown in Figure S1A,B follows the PCA results, i.e. the amount of data variance explained by each map decreases from left to right. Using standard microstate labelling, the maps from left to right would be labelled B, A, D, C. For analytic amplitude and phase microstates, the standard labelling does not apply. In sum, alpha band-pass microstates are highly similar to full bandwidth (1-30 Hz) microstates. Amplitude and phase microstates do not necessarily follow standard microstate geometries, but do form large-scale structures.

Stuart-Landau lattice autoinformation functions

In the main text, we only showed the AIFs for the critical Stuart-Landau system (Figure 8). We here add the cases where the bifurcation parameter μ is (i) well below the bifurcation point ($\mu = -1.0$), and (ii) above the bifurcation point ($\mu = 1.0$). For completeness, we repeat the AIFs at the bifurcation point ($\mu = 0.0$). The results are summarized in Figure S2. Below the bifurcation point (Figure S2A), the individual oscillators show a weak oscillatory behaviour due to the noise included in the simulation (noise-induced oscillations), leading to small peaks at time lags $t = \pi$ (half-cycle) and $t = 2\pi$ (full cycle length, gray vertical line) in the AIF of oscillation-derived microstates (black). These peaks are weakly present in the phase-derived microstates (green) but not in the analytic amplitude microstate AIF (blue). As the oscillators do not form coherent large-scale structures, the amplitude AIF is flat, indicating small memory effects in amplitude-derived microstate sequences.

Figure S2B shows the AIF curves for $\mu = 0$ (same as Figure 8E), qualitatively similar to the actual EEG data. In particular, oscillation-derived microstates (black) show multiple, but decaying periodic peaks that are reproduced by the phase-derived microstate sequence (green), but not by amplitude microstates

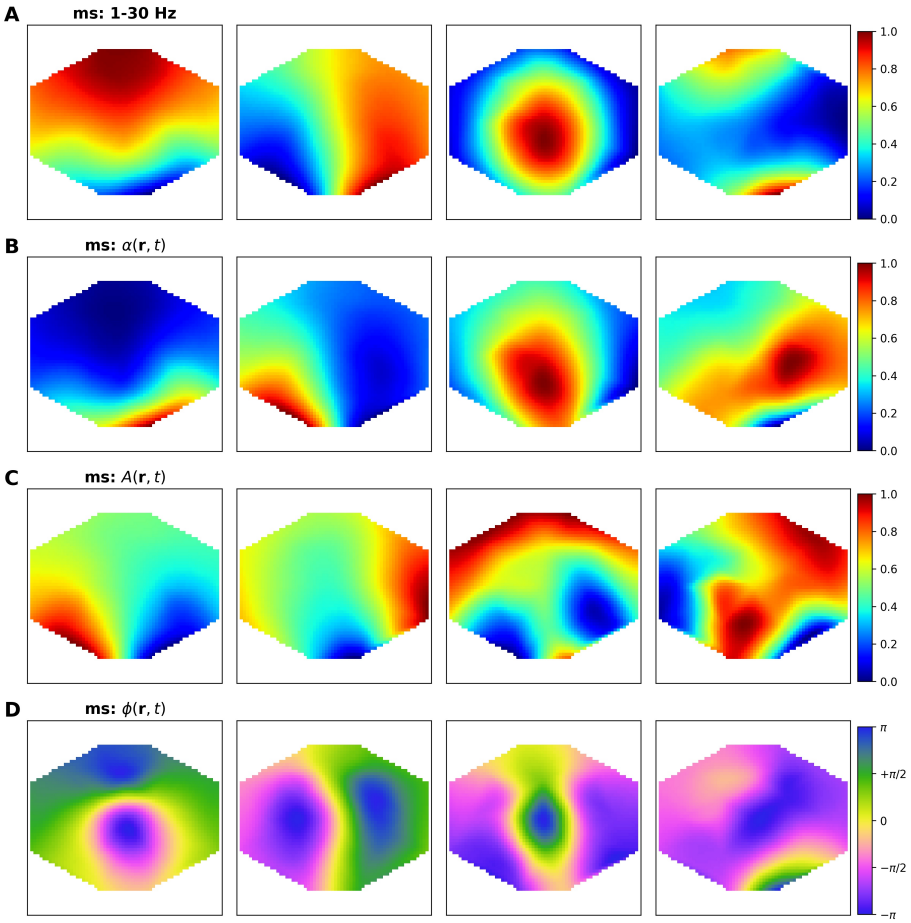

Figure S1: Single subject microstate maps. **A**: Microstate maps from 1-30 Hz EEG data. **B**: Microstate maps from 8-12 Hz alpha band data. **C**: Microstate maps from analytic alpha amplitude data. **D**: Microstate maps from analytic alpha phase data.

(blue). The latter show large and slowly decaying AIF coefficients compared to Figure S2A, indicating strong memory effects.

Figure S2C illustrates the results above the bifurcation point ($\mu = 1.0$), where all oscillators produce steady oscillations of constant amplitude, waveforms that are never observed in real EEG. Accordingly, oscillation- and phase-derived microstate sequences show a non-modulated periodic behaviour with recurring, non-decaying periodic AIFs (black, green). As the complex amplitude in this case is constant ($A(\mathbf{r}, t) = 1$ for all $\mathbf{r}, t$), there is only one spatial pattern that would correspond to a flat EEG topography of constant amplitude. In this case, the microstate algorithm does not give useful results, however, carrying out the subsequent calculations yields the flat AIF in Figure S2C (blue).

Phase rotor animations

The following files contain animations of the data shown in Figures 2, 3, 4, 5, 8 of the main text. Detailed descriptions of these dynamic patterns are given in the main body of the manuscript.

- The data shown in Figure 2 are animated in Mov1_Fig_2.
- The data shown in Figure 3 are animated in Mov2_Fig_3.
- The data shown in Figure 4 are animated in Mov3_Fig_4.
- The data shown in Figure 5 are animated in Mov4_Fig_5.
- The Stuart-Landau lattice example shown in Figure 8A is animated in Mov5_CSLE_S1, Figure 8B in Mov6_CSLE_S2.

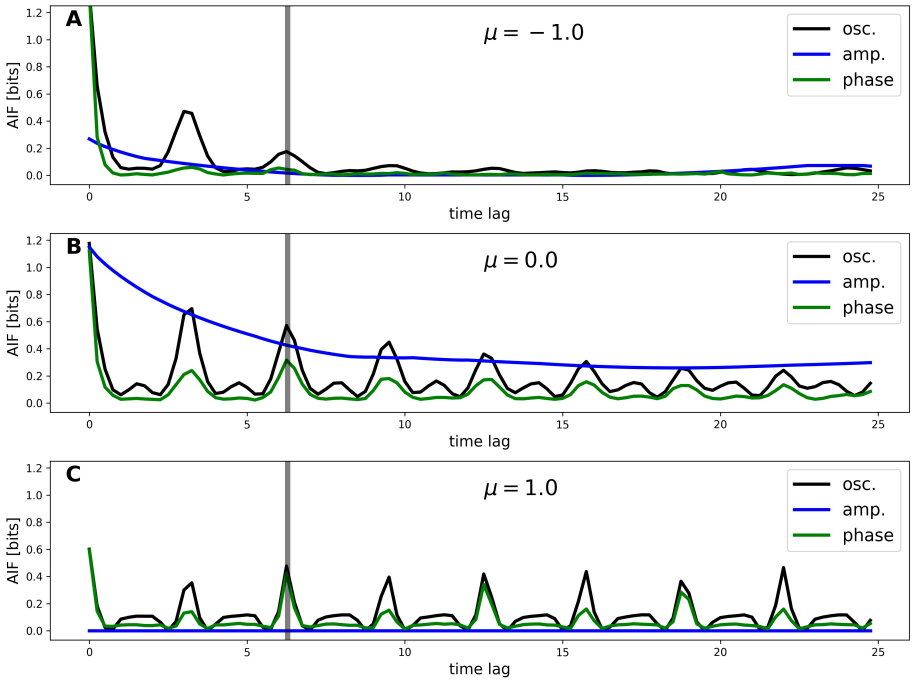

Figure S2: Autoinformation functions (AIF) for the Stuart-Landau oscillator model system for different control parameter settings. AIFs are shown for microstates derived from the band-pass filtered oscillations (black), their analytic amplitude (blue) and analytic phase (green). The Stuart-Landau cycle length (time lag $t = 2\pi$) is indicated by a vertical gray line in A-C. **A**: At $\mu = -1.0$, oscillation- and phase-derived microstates (black, green) have a weak periodic component due to noise-induced oscillations below the bifurcation point. Amplitude microstates (blue) are not periodic and show only minimal memory effects compared to B. **B**: At the bifurcation point ($\mu = 0.0$), oscillation microstate periodicity (black) extends to large time lags and is followed by the AIF of phase-derived microstates (green). Amplitude microstates show long lasting memory effects with a larger amplitude than in A for all time lags. **C**: AIFs above the bifurcation point ($\mu = 1.0$) show non-decaying periodicities for oscillation- and phase-derived microstates (black, green). For $\mu = 1.0$, all oscillators show non-modulated (fixed-amplitude) oscillations. In this case, there is only one (constant) microstate, such that subsequent computations fail, leading to a flat AIF (blue).

Table S1: Microstate parameters (I) for all n=23 subjects. Peaks-per-second (PPS) in the global field power (GFP) time courses of 1-30 Hz EEG data ($PPS_{1\text{-}30}$) and alpha band filtered data ($PPS_{8\text{-}12}$), Global explained variance by four microstates computed from 1-30 Hz data ($GEV_{1\text{-}30}$). EV: variance explained by four PCA-derived microstates calculated from 1-30 Hz data ($EV_{1\text{-}30}$), alpha oscillations ($EV_{8\text{-}12}$), analytic alpha amplitude (EV_A), and analytic alpha phase (EV_ϕ). All variances in %/100.

Subj. #	$PPS_{1\text{-}30}$	$PPS_{8\text{-}12}$	$GEV_{1\text{-}30}$	$EV_{1\text{-}30}$	$EV_{8\text{-}12}$	EV_A	EV_ϕ
0	24.87	20.90	0.61	0.90	0.94	0.82	0.90
1	25.08	20.27	0.56	0.85	0.93	0.73	0.85
2	24.20	19.90	0.57	0.87	0.95	0.83	0.87
3	25.41	21.50	0.58	0.89	0.93	0.66	0.89
4	25.57	20.85	0.60	0.90	0.94	0.76	0.90
5	21.93	18.81	0.60	0.90	0.97	0.88	0.90
6	23.23	20.97	0.64	0.91	0.97	0.86	0.91
7	20.63	19.07	0.64	0.93	0.97	0.80	0.93
8	23.69	19.49	0.58	0.88	0.93	0.67	0.88
9	23.96	20.82	0.59	0.89	0.95	0.83	0.89
10	27.39	22.11	0.64	0.91	0.95	0.74	0.91
11	23.06	20.90	0.64	0.93	0.96	0.78	0.93
12	22.57	18.74	0.58	0.89	0.94	0.75	0.89
13	23.89	20.37	0.67	0.93	0.97	0.85	0.93
14	21.95	20.18	0.62	0.92	0.97	0.89	0.92
15	25.91	18.73	0.56	0.84	0.93	0.68	0.84
16	22.98	19.84	0.68	0.94	0.99	0.89	0.94
17	23.89	20.62	0.58	0.88	0.94	0.79	0.88
18	28.28	22.03	0.53	0.83	0.89	0.70	0.83
19	20.98	18.42	0.72	0.95	0.98	0.88	0.95
20	24.52	20.51	0.59	0.89	0.95	0.79	0.89
21	29.38	21.07	0.58	0.87	0.92	0.69	0.87
22	20.82	19.32	0.62	0.92	0.97	0.85	0.92

Table S2: Microstate parameters (II) for all n=23 subjects. Shannon entropy H in nats ($\log_e$) for microstate sequences computed from 1-30 Hz EEG data ($H_{\text{1-30}}$), alpha oscillations ($H_{\text{8-12}}$), the analytic alpha amplitude (H_A) and the analytic alpha phase (H_ϕ). The mixing times τ of the microstate transition matrix computed at a sampling rate of 250 Hz for 1-30 Hz data ($\tau_{\text{1-30}}$), alpha oscillations ($\tau_{\text{8-12}}$), analytic alpha amplitude (τ_A), and analytic alpha phase (τ_ϕ).

Subj. #	$H_{\text{1-30}}$	$H_{\text{8-12}}$	H_A	H_ϕ	$\tau_{\text{1-30}}$	$\tau_{\text{8-12}}$	τ_A	τ_ϕ
0	1.17	1.09	1.03	1.21	3.35	3.34	41.79	3.39
1	1.18	1.10	1.20	1.11	3.80	3.56	30.92	3.41
2	1.24	1.15	1.15	1.09	3.63	3.83	48.52	3.37
3	1.21	1.20	1.33	1.15	3.58	3.63	29.63	3.42
4	1.17	1.08	1.09	1.14	3.27	3.44	29.09	3.40
5	1.20	1.06	1.34	1.15	4.00	3.76	35.53	4.02
6	1.17	1.11	1.25	1.16	3.69	3.53	30.54	3.47
7	1.15	1.05	0.79	1.13	3.99	3.72	39.78	3.91
8	1.18	1.11	1.33	1.15	3.61	3.73	32.65	3.70
9	1.21	1.18	1.32	1.13	3.73	3.80	37.59	3.29
10	1.13	1.05	1.20	1.04	3.09	3.10	22.11	3.17
11	1.15	1.10	1.27	1.02	3.56	3.63	35.68	3.45
12	1.22	1.12	1.22	1.14	4.13	3.79	32.91	3.61
13	1.09	1.00	0.89	1.15	3.36	3.33	36.65	3.62
14	1.14	1.00	0.90	1.18	3.58	3.33	55.94	3.91
15	1.21	1.16	1.34	1.11	4.13	4.14	27.72	3.49
16	1.07	0.96	1.14	0.94	3.58	3.52	55.22	3.35
17	1.22	1.04	1.23	1.17	3.86	3.24	30.37	3.55
18	1.23	1.23	1.38	1.21	3.23	3.65	24.03	3.40
19	0.97	0.82	0.44	1.11	3.36	3.03	41.23	3.44
20	1.19	1.09	1.33	1.16	3.48	3.70	32.93	3.73
21	1.17	1.16	1.27	1.19	3.07	3.65	21.22	3.49
22	1.17	1.08	0.81	1.07	4.01	3.75	40.04	3.94